

## WIRELESSLY POWERING: THE FUTURE

# Methodology for the design of multi-source transmitters dedicated to perpendicular dynamic wireless power transfer: theoretical study

LOTFI BEGHOU

*In this paper, a theoretical study for the design of multi-source transmitters suitable for perpendicular dynamic wireless power transfer is presented. Unlike conventional systems, the concept presented here overcomes the traditional limitation on the receiver's orientation by providing an optimal distribution of the transmitted energy obtained by using different sources. For this purpose, a theoretical study of different transmitters has been achieved by solving the inverse problem. Comparison with conventional single-source transmitters carrying the same total current as the multi-source transmitters, shows a significant enhancement of the power gain when a Genetic Algorithm is used. The obtained theoretical results show power gain levels over 7.5 dB for different path lengths at different heights. At the end, a solution for a path of an infinite length is presented.*

**Keywords:** Wireless power transfer, Inverse problem, Genetic Algorithm

Received 19 May 2017; Revised 9 September 2017; Accepted 29 November 2017; first published online 21 January 2018

## I. INTRODUCTION

Power integration in every day's life activities is in a constant increase and more particularly in areas where standalone devices require very high-power density levels. Many research works have been oriented toward integration solutions especially in the fields of MEMS and wireless sensor networks. However, these devices still require a power source, which allows them to function. One straightforward solution for energy harvesting in such applications is the micro-battery [1] of which the specific capacity is a crucial parameter. In the meantime, the idea of battery-less systems, where power is supplied to the device wirelessly, using the concept of wireless power transfer (WPT) [2], has made some way further from theory and closer to practicality. In such systems, space allocated to the stated above power sources is saved and consequently device mobility is increased. Many types of WPT systems have been studied so far, in the far-field region energy can be transmitted via microwaves [3, 4], while inductive coupling [5, 6] and capacitive coupling [7, 8] allow WPT in the near-field region. The concept presented here is an inductive coupling-based system allowing WPT in the near-field region. However, although WPT saves the

space allocated to the onboard power source, it is known that such a concept faces serious limitations especially when the distance separating both transmitter and receiver gets to increase. At this matter, authors in [9] realized a comparative study showing the effect of area difference as well as transmitter-to-receiver distance on WPT efficiency. At this matter, it is important to know that many medical applications with standalone devices placed within the body require a power transfer through a transmitter-to-receiver distance of few centimeters with a variable receiver orientation [10, 11], especially when the receiver gets to move along a given path as in [12].

In order to solve these problems, the system presented in this paper is a multi-source transmitter for dynamic WPT dedicated to applications where the receiver is in motion along a given path and where transmitter-to-receiver relative shift-angle is constraining. At this matter, many research works on insensitive transmitter's orientation have been developed. In [13], authors have presented an adaptive method to improve the efficiency of WPT systems with axial misalignment. The proposed system achieved a relative efficiency improvement of 48.5% but only for axial misalignment. In [14], a detailed theoretical and numerical analyses of resonant magnetic coupling to address misalignment between the transmitter and the receiver is achieved. For this purpose, formulae are derived for the magnetic field of the receiver coil when it is laterally and angularly misaligned from the receiver. Even though, the previous works show interesting results, three-dimensional (3D) transmitters remain the best solution

Electrical and Computer Engineering, University of British Columbia, Vancouver, British Columbia, Canada V6T 1Z4

**Corresponding author:**

L. Beghou

Email: lotfi.beghou@gmail.com

for axial and angular misalignment problem. For instance, authors in [15] have developed an optimized three-loop misalignment structure for WPT via strong coupled magnetic resonance (SCMR). Obtained results show efficiency levels of 60% while typical SCMR in WPT application show efficiency level lower than 10%. While in [16], authors have developed a non-identical current control for 2D and 3D omnidirectional wireless power transmitters. Obtained results show efficiency levels higher than 50%. At the difference of systems developed in [15, 16], the system presented here is an association of magnetic field sources of which orientations are optimized using a Genetic Algorithm (GA). The obtained optimum corresponds to the configuration, which provides a power transfer with a minimum energy amount at the transmitter side. In [17], authors have investigated inductive coupling WPT for RFID (Radio Frequency Identification) transponders enabling an optimized system design. For this purpose, a modified PEEC (Partial Elements Equivalent Circuit) method is derived based on antenna parameters such as geometries, mutual inductance, and resistance. In the work presented here, an inverse-problem-based method is used to characterize the magnetic field emitted from the set of sources which have the same geometry and location but with a different current distribution. Details on the system and design procedure are presented in the following sections with emphasis on the optimization process. Theoretical results are presented at the end of the paper with a loss discussion about the converter which could be associated with the designed multi-source transmitter. Finally, it is important to mention that no experimental validation has been carried on the presented concept. Regarding this, a finite element's simulation has been achieved in order to validate the used model within the considered frequency range. This minimizes the risk of unexpected real-life aspects that may not have been taken into account during this study.

## II. THE MULTI-SOURCES SYSTEM

To illustrate how WPT works, a receiver is placed in different configurations at a given distance with a given orientation, above a conventional flat transmitter represented by a single turn coil.

The effect of receiver's disposition on the WPT efficiency is expressed by the coupling factor of which the value describes

the amount of energy transferred from a transmitter toward a receiver:

$$k = \frac{\varnothing_r}{\varnothing_t} = \frac{n_r \oint B_r \cos(\theta_r) \cdot \partial A_r}{n_t \oint B_t \cdot \partial A_t}, \quad (1)$$

where  $B_r$  is the received magnetic flux density at a given point across the receiver area;  $\theta_r$  is the receiver orientation angle;  $n_r$  the number of turns at the receiver;  $A_r$  the receiver cross-sectional area. Terms with the subscripts "t" correspond to the transmitter side.

Figure 1(a) shows a conventional system where both transmitter and receiver have similar areas and are placed close to each other. Such a configuration provides a magnetic flux density more or less constant over  $A_r$  and the magnetic field lines are parallel to the receiver's axis. Consequently, equation (1) becomes

$$k_1 = \frac{n_r \oint B_r \cdot \partial A_r}{n_t \oint B_t \cdot \partial A_t}. \quad (2)$$

By applying equation (1) to the configuration presented in Fig. 1(b) the coupling factor becomes:

$$k_1 = \frac{\varnothing_r}{\varnothing_t} = \frac{n_r \oint B_r \cos(90^\circ) \cdot \partial A_r}{n_t \oint B_t \cdot \partial A_t} = 0. \quad (3)$$

In other words, the receiver's does not collect any field line and there will be no power transferred to the receiver. The comparative study in [9] shows how the area difference between the transmitter and the receiver as well as the distance separating them affects the coupling factor value. For this purpose, the authors have considered concentric and flat coils for both transmitter and receiver. However, as soon as the receiver starts moving as in [12], the leakage field intensity increases and the magnetic flux density becomes a function of the  $x$ -coordinate.

Figure 2 shows a rough distribution of magnetic field lines between two points A and B and where a receiver similar to the one in [12] is moving back and forth. It can be observed that the induced *emf* varies according to the receiver's position and decreases each time the receiver approaches the center

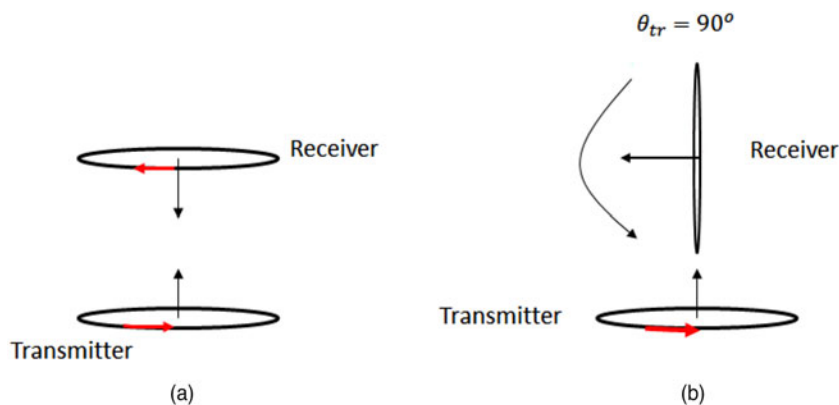


Fig. 1. (a) Conventional receiver disposition, (b) our receiver disposition.

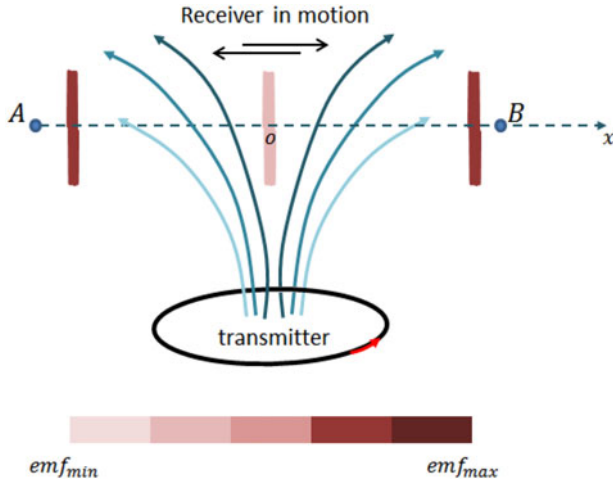


Fig. 2. Magnetic field lines along a non-parallel oriented path.

“ $o$ ”. The coupling factor expression becomes:

$$k_3 = \frac{n_1 \oiint B(x) \cdot \cos(\theta_r) \cdot \partial A_r}{n_t \oiint B_t \cdot \partial A_t} \ll k_3. \quad (4)$$

The WPT system studied in this paper is dedicated to applications where the shift angle between transmitter and receiver

respective axes is constraining. For this purpose, the proposed transmitter topology presented here is shown in Fig. 3. Such a topology allows a more efficient energy re-distribution so that the receiver always sees the same magnetic flux.

The transmitter-to-receiver distance of the multi-source transmitter  $d_{tr_1}$  is expressed as following:  $d_{tr_1} = d_{tr_2} + \max(r_i \cdot \sin(\theta_i))$ ; where  $r_i$  is the source  $i$  radius;  $d_{tr_2}$  is the transmitter-to-receiver distance of a conventional transmitter;  $\theta_i$  is the source  $i$  spherical orientation angle shown in Fig. 4. For the design of such systems, the inverse problem widely used in electromagnetic characterization is solved. This gives the sources currents needed to provide the required magnetic field value along the receiver’s path (with minimum transmitted energy). Then, obtained systems are compared with the conventional single-source flat transmitters. At this matter, it is worth it to mention that the total current injected in a multi-source transmitter is the same current injected in one conventional transmitter.

### III. SYSTEM DESIGN

In this paper, a design methodology for more efficient perpendicular WPT systems is presented. For this purpose an inverse problem-based characterization method is used and where the parameters of each source are obtained by minimizing

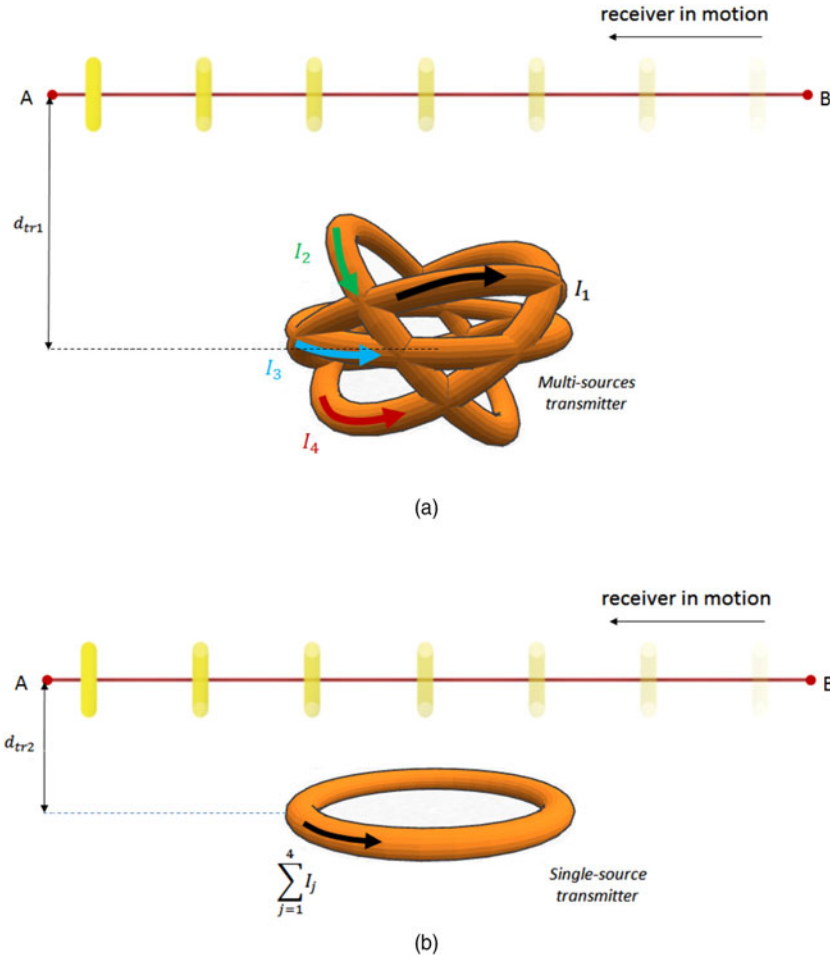


Fig. 3. (a) Receiver in motion above a concentric multi-source transmitter, (b) receiver in motion above a conventional transmitter.

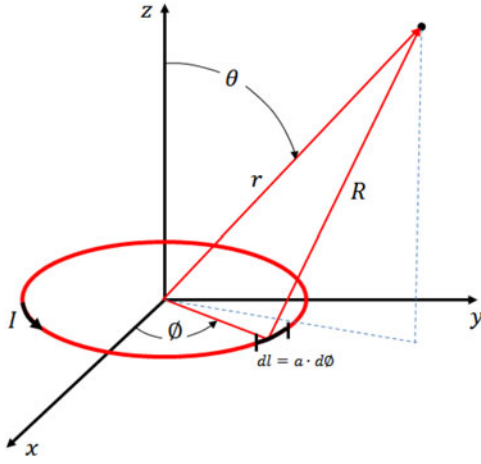


Fig. 4. Magnetic dipole.

the error between the total magnetic field emitted by the transmitter in question and the magnetic field needed along the receiver's path. The function describing this error is expressed as follows:

$$\varepsilon(\vec{P}) = \sum_{j=1}^{N_p} \vec{H}_{mod}^j - \vec{H}_{def}^j, \quad (5)$$

$\vec{H}_{mod}^j$  is the magnetic field emitted by the transmitter's model at point  $J$ ;  $\vec{H}_{def}^j$  is the magnetic field defined at point  $J$ ;  $\vec{P}$  is the parameters vector;  $\varepsilon$  the fitness function representing the minimized error). In order to maximize the coupling factor, the magnetic field component parallel to the receiver's path must be the same along the entire receiver's path. To achieve this, a number of calculation points  $N_p$  is considered and along which the fitness function  $\varepsilon(\vec{P})$  is minimized in terms of the parameters vector  $\vec{P}$ .

### A) The characterization method

As stated above, the key point in this work consists of finding a better energy distribution by using different sources rather than one source as it is the case in conventional transmitters. The model used to predict the magnetic field distribution for such a configuration and which assumes a constant current along the source is the magnetic dipole, which is based on Legendre functions:

Thus, the source circumference must remain well below the wavelength (here  $2\pi \cdot a \leq (\lambda/20)$ ;  $a$  is the dipole radius). Thus, the magnetic field emitted by the magnetic dipole "i" at a point "j" along the receiver's path is described as follows [18]:

$$\vec{H}_{modj}^i = B_{LGj}^i \cdot B_{CCj}^i \cdot \vec{H}_{cylj}^i. \quad (6)$$

Where

$$\vec{H}_{cylj}^i = \begin{bmatrix} \frac{k \cdot z'_j}{4\pi \cdot \rho'_j \cdot \sqrt{a \cdot \rho'_j}} \left[ -L_1 + \frac{a^2 + \rho_j'^2 + z_j'^2}{(a - \rho_j')^2 + z_j'^2} L_2 \right] \\ 0 \\ \frac{k}{4\pi \sqrt{a \cdot \rho'_j}} \left[ L_1 + \frac{a^2 - \rho_j'^2 - z_j'^2}{(a - \rho_j')^2 + z_j'^2} L_2 \right] \end{bmatrix} \times I^i$$

is the magnetic field in a cylindrical local-coordinates system and where  $L_1$  and  $L_2$  are Legendre functions [19].  $B_{LG}$  is the transformation matrix from local to global coordinates system and  $B_{CC}$  is the transformation matrix from cylindrical to Cartesian coordinates and  $I^i$  is the current in source  $i$ . Then, if we write the magnetic field as:

$$\vec{H}_{modj}^i = A_j^i \cdot I^i. \quad (7)$$

With the expression of matrix  $A_j^i$ :

$$A_j^i = B_{LGj}^i \cdot B_{CCj}^i \begin{bmatrix} \frac{k \cdot z'_j}{4\pi \cdot \rho'_j \cdot \sqrt{a \cdot \rho'_j}} \left[ -L_1 + \frac{a^2 + \rho_j'^2 + z_j'^2}{(a - \rho_j')^2 + z_j'^2} L_2 \right] \\ 0 \\ \frac{k}{4\pi \sqrt{a \cdot \rho'_j}} \left[ L_1 + \frac{a^2 - \rho_j'^2 - z_j'^2}{(a - \rho_j')^2 + z_j'^2} L_2 \right] \end{bmatrix};$$

and the total magnetic field emitted by the set of  $N$  sources at the same point  $J$  is expressed as:

$$\vec{H}_{modj} = \sum_{i=1}^N A_j^i \cdot I^i. \quad (8)$$

The magnetic field emitted at  $P$  points along the receiver's path becomes then:

$$\vec{H}_{mod} = [\vec{H}_{mod_1} \cdots \vec{H}_{mod_p}]. \quad (9)$$

$$\vec{H}_{mod} = \begin{bmatrix} \sum_{i=1}^N A_1^i|_x \cdot I^i & \sum_{i=1}^N A_2^i|_x \cdot I^i & \cdots & \sum_{i=1}^N A_p^i|_x \cdot I^i \\ \sum_{i=1}^N A_1^i|_y \cdot I^i & \sum_{i=1}^N A_2^i|_y \cdot I^i & \cdots & \sum_{i=1}^N A_p^i|_y \cdot I^i \\ \sum_{i=1}^N A_1^i|_z \cdot I^i & \sum_{i=1}^N A_2^i|_z \cdot I^i & \cdots & \sum_{i=1}^N A_p^i|_z \cdot I^i \end{bmatrix}. \quad (10)$$

Such an equation provides a system with  $3P$  equations:

$$\left\{ \begin{array}{l} \vec{H}_{mod_1}|_x = A_1^1|_x I^1 + A_2^1|_x I^2 + \dots + A_1^N|_x I^N \\ \vec{H}_{mod_1}|_y = A_1^1|_y I^1 + A_2^1|_y I^2 + \dots + A_1^N|_y I^N \\ \vec{H}_{mod_1}|_z = A_1^1|_z I^1 + A_2^1|_z I^2 + \dots + A_1^N|_z I^N \\ \vdots \\ \vec{H}_{mod_p}|_x = A_1^p|_x I^1 + A_2^p|_x I^2 + \dots + A_1^N|_x I^N \\ \vec{H}_{mod_p}|_y = A_1^p|_y I^1 + A_2^p|_y I^2 + \dots + A_1^N|_y I^N \\ \vec{H}_{mod_p}|_z = A_1^p|_z I^1 + A_2^p|_z I^2 + \dots + A_1^N|_z I^N \end{array} \right. \quad (11)$$

While only  $N$  equations are required to solve this problem. This is why the number of available equations must be  $3P \geq N$ . However, by assuming the receiver's path to be parallel to the  $x$ -coordinates axis, we notice that only the  $x$ -component

$\vec{H}_x$  of the magnetic field contributes to *emf* induction:

$$emf = -\frac{d(B_x(t) \cdot A_r)}{dt}, \quad (12)$$

where *emf*: electromotive force or induced voltage across the receiver;  $B_x(t)$  is the average magnetic flux density over the receiver's area in the time domain;  $A_r$  is the receiver's area.

Thus, only the *x*-component  $\vec{H}_{def\ x}$  has to be set for the problem resolution; and equations related to *z*- and *y*-components are not needed anymore. Moreover, including them requires setting values for  $\vec{H}_{def\ x,y}$  which will considerably reduce the solutions space. This is why a number of calculation points  $P=N$  is considered to provide enough equations for problem resolution. Thus, the sources current vector is obtained by achieving the following operation:

$$\vec{I} = A^{-1} \cdot \vec{H}_{mod}|_x. \quad (13)$$

With

$$A = \begin{bmatrix} A_1^1|_x & \dots & A_1^N|_x \\ \vdots & \dots & \vdots \\ A_p^1|_x & \dots & A_p^N|_x \end{bmatrix}.$$

Thus, by considering the ideal case, the expression of the sources current vector becomes:

$$\vec{I} = \begin{bmatrix} I_1 \\ I_2 \\ \vdots \\ I_N \end{bmatrix} = \begin{bmatrix} A_1^1|_x & \dots & A_1^N|_x \\ \vdots & \dots & \vdots \\ A_p^1|_x & \dots & A_p^N|_x \end{bmatrix}^{-1} \times \begin{bmatrix} H_{def}^1 \\ H_{def}^2 \\ \vdots \\ H_{def}^N \end{bmatrix}. \quad (14)$$

The elements constituting this current vector represent the different currents to be injected in the corresponding magnetic field sources.

## B) The optimization

In this work, spherical orientation angles  $\phi$  and  $\theta$  have been considered as optimization parameters. These parameters bring a non-linear behavior to the magnetic field expression and make the fitness function in equation (5) full of local optimums, especially when the number of sources becomes important. For this purpose, a simple GA which is a stochastic global optimization method is used to minimize the fitness function given in equation (5). In [20], it is shown that the higher is the scheme's order; the lower is its survival probability. In addition, it remains very important not to exceed the maximum mutation probability which is a function of the precision required for each optimization parameter:

$$prob_{mut} < prob_{mut\ max} = \frac{1}{l_i}. \quad (15)$$

$prob_{mut\ max}$  the maximum mutation probability,  $l_i$  the length of individuals in the population). Then, optimization is performed by assuming a minimum energy constraint under

which the total current delivered to the multi-source transmitter is minimized  $min(sum\ \vec{I})$ . At the end of the process, source currents are obtained for the optimum orientation angles  $\theta$  and  $\varphi$ . For a set of six sources, the precision required for each parameter has been set to  $0.17^\circ$  for  $\theta$  and  $0.35^\circ$  for  $\varphi$  which leads to a maximum mutation probability of  $p_{mu\ max} = 0.0083$ . If  $p_{mu} = p_{mu\ max}$  all population individuals will undergo mutation. In order to preserve the population evolution, it has been decided that only 10% of the population undergoes the mutation. Thus  $p_{mu} = p_{mu\ max} \cdot 10\%$  and cross-over probability is set to  $p_{cross} = 0.7$ . Table 1 shows the different dimensions, path lengths and heights for which system design has been achieved. (Here the term height refers to the *z*-coordinate of the receiver's path if we assume that this path is parallel to the *x*-coordinate axis as shown in Fig. 5.)

Optimization results presented in this section correspond to systems designed to provide a magnetic field with a magnitude of 2 A/m along the receiver's path. Here, a receiver with a radius of 4 mm similar to those found in micro-robots applications is considered. Table 2 shows the parameters of the designed systems when a path of 8 cm is considered. For this purpose, only systems using sets of six sources are presented (parameters listed in the table are shown in Fig. 4):

The topology of the multi-source transmitter corresponding to the first line of Table 2 is shown in Fig. 4:

Table 3 shows the parameters of the designed systems when a path of 12 cm is considered (parameters listed in the table are shown in Fig. 4).

## C) Model's frequency limit

The validity of the model proposed here depends on both frequency and distance. These two parameters are involved in the expression of the magnetic potential vector:

$$\vec{A} = \frac{\mu_0}{4\pi} \int_l \frac{\vec{i}(r)}{R} e^{-jkR} dl, \quad (16)$$

where  $k = (2\pi/\lambda)$  is the wave number and  $\lambda$  is the wavelength.

The frequency which is present in the exponential term  $e^{-jkR}$  makes the calculation of the integral above impossible for a magnetic dipole. However, the evolution of this term shows that for a given maximum source-to-receiver distance  $real(e^{-jkR}) \approx 1$  as long as the operation frequency is lower than the frequency limit. While for higher frequencies, the real part starts decreasing and introduces an error in the magnetic field estimation. Consequently, the model's frequency limit will be represented by the green line in Figs 8–11 of which the values have been obtained according to the  $kR$  coefficient expression:

**Table 1.** Design conditions

Height $d_{tr2}$	3 cm	4 cm	5 cm
Path length	8 & 12 cm	8 & 12 cm	8 & 12 cm
Source radius	6 & 8 cm	6 & 8 cm	6 & 8 cm

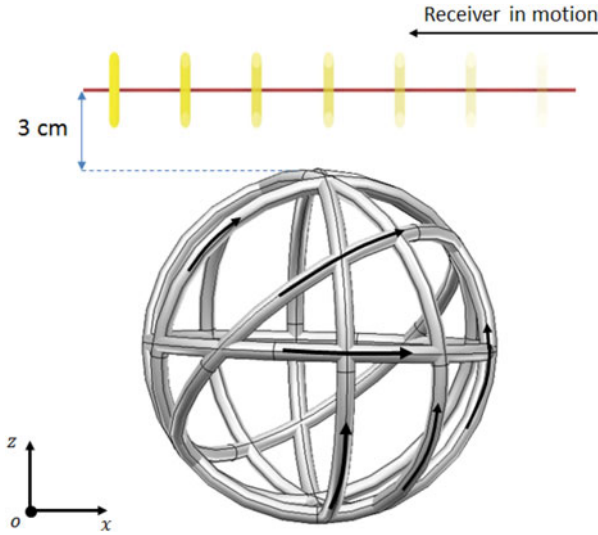


Fig. 5. Transmitter topology.

$$kR = \frac{2\pi}{\lambda} \cdot \max \left( \sqrt{(z + 2 \cdot r_s \cdot \sin(\theta))^2 + \left( r_s \cdot \cos(\theta) + \frac{l_p}{2} \right)^2} \right) = 0.001, \quad (17)$$

where  $z$  is the receiver height,  $r_s$  is the source radius, and  $l_p$  is the path length.

Thus, the frequency limit for a 6 cm radius transmitter placed at 5 cm from the receiver's path is equal to 2.15 MHz. Model validation of this configuration has been achieved using the FEA tool COMSOL for a transmitter of a 6 cm radius and 1 A current. The emitted magnetic field norm has been compared at a distance of  $z = 5$  cm and a path length of 50 cm along the  $x$ -axis (Fig. 6):

This comparison shows clearly that the suggested model in Section II is usable and results presented in the following section can be considered as reliable.

#### IV. DESIGN RESULTS

Receiver's dimensions in medical applications are usually small compared with the transmitter's size. Thus according to equation (1), the coupling factor (WPT efficiency) will drastically fall. This is why, in order to estimate the performance of the designed systems, the single-source-to-multi-source power gain has been estimated. Figure 8 shows this gain evolution when sources have a radius of 6 cm:

$$G_{dB} = 10 \cdot \log \left( \frac{P_m}{P_s} \right) = 20 \cdot \log \left( \frac{V_m}{V_s} \right) \quad (18)$$

$P_m$  and  $V_m$  are respectively the power and the voltage across the load when using a multi-source transmitter. While the same terms with the subscript "s" correspond to the single-source transmitter. The receiver's equivalent circuits in both configurations are presented in the figure below (Fig. 7):

By neglecting the receiver's coil resistance  $r_r$  the voltage across the load becomes:  $V_m = emf_m$  and  $V_s = emf_s$ . By considering sinusoidal currents at the transmitter, the induced  $emf$  can be written:

$$emf_m = -j\omega \cdot B_m \cdot \cos(\theta_m) \cdot A \quad (19)$$

and

$$emf_s = -j\omega \cdot B_s \cdot \cos(\theta_s) \cdot A.$$

By considering the receiver path parallel to (ox):

$$emf_m = -j\omega \cdot B_{mx} \cdot A = V_m \quad (20)$$

Table 2. The transmitter's parameters

	Height (cm)	Orientation angle $\theta$ [rad]	Orientation angle $\varphi$ [rad]	Current sum (A)
Sources radius 6 cm	3	[1.81, 1.57,0.8,1.5,1.37,0.11]	[1.57,0.19,2.5,0.82,1.37]	0.3087
	4	[1.71,1.6,1.67,1.69,1.19,0.06]	[0.4,1.76,0.9,0.12,0.83,1.08]	0.2974
	5	[1.8,1.65,0.88,1.57,1.29,0.015]	[0.46,0.8,1.61,3.36,1.96,0.036]	0.2937
Sources radius 8 cm	3	[1.58,1.71,1.57,1.67,1.68,0.4]	[1,3.84,0.25,4.9,1.633,62]	0.3419
	4	[1.13,2,1.2,0.8,1.57,0]	[1.1,1,08,5,6,1.5,2.5]	0.3839
	5	[1.96,1.59,1.53,0.2]	[3.84,0.61,1.57,0.78]	0.3597

Table 3. The transmitter's parameters

	Height (cm)	Orientation angle $\theta$ [rad]	Orientation angle $\varphi$ [rad]	Current sum (A)
Sources radius 6 cm	3	[1, 1, 8,1.77,1.8,1.6,0]	[0.85,4,1.57,0.90,2,1]	0.2863
	4	[0.74,1.78,1.57,1.4,0.6,0]	[1.6,2.3,0.25,4.32,1.2,3.24]	0.778
	5	[0.6,1.8,1.2,1.572,2.56,0]	[1.2, 2.62,2,1.57,1.6,0]	1.26
Sources radius 8 cm	3	[1.57,1.67,1.6,1.63,1.38,0.4]	[3.24,0.71,4.12,1.65,1.51,1.64]	0.3473
	4	[1.57,0.78,0.81,1.78,1.57,0.13]	[0.82,5.22,0.95,0.24,1.87,0]	0.3297
	5	[1.96,1.2,1.6,0.78,1.66,0]	[0.32,4.72,0.4,2,4.76,0]	0.3626

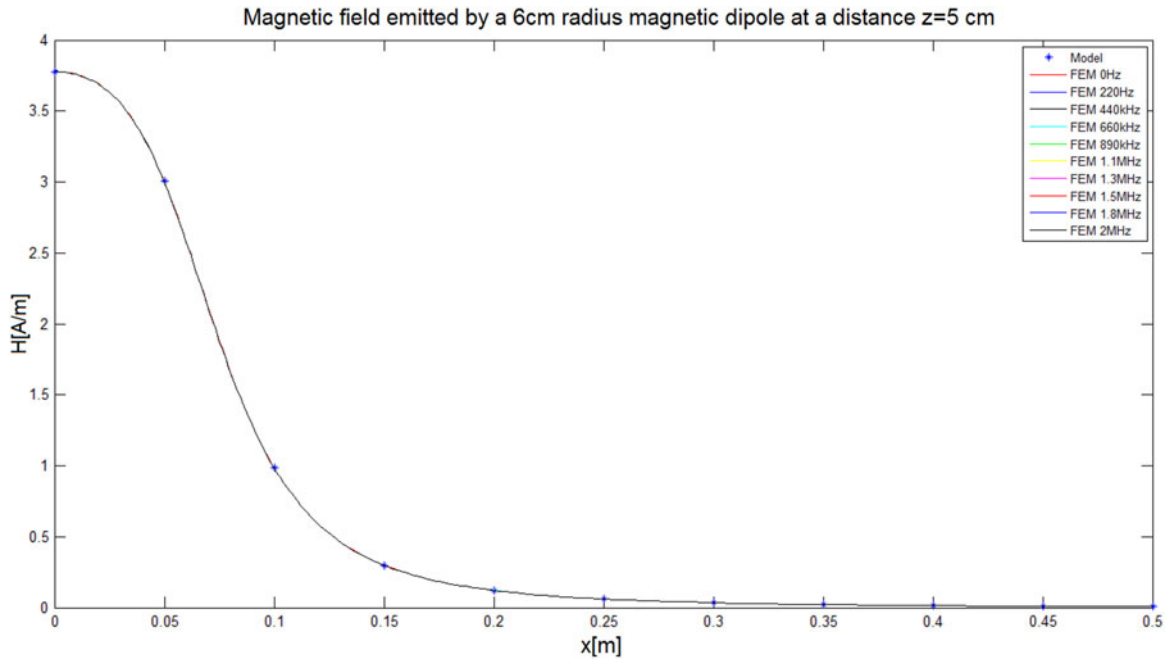


Fig. 6. Magnetic field norm emitted at a distance of  $z = 5$  cm along a 50 cm path length using both model and finite elements simulation for a frequency range going from 0 Hz to 2 MHz.

and

$$emf_s = -j\omega \cdot B_{sx} \cdot A = V_s. \quad (21)$$

For gain estimation, the power is calculated for transmitters with the same radius. However, the current injected within the single-source conventional transmitter is equal to the sum of the currents flowing in each source of the multi-source transmitter:

$$G_{dB} = 20 \cdot \log\left(\frac{B_{mx}}{B_{sx}}\right). \quad (22)$$

Figure 8 shows the gain evolution obtained with transmitters containing six sources of 6 cm radius each along an 8 cm length path in terms of its height. It shows clearly how a set of sources improves the power transfer. For instance, we observe that the power gain is enhanced up to 14 dB at a height of 5 cm when a multi-source transmitter is used. The green line represents the frequency limit of the transmitter’s model.

While Fig. 9 shows the evolution of the power gain as well as the frequency limit for transmitters containing six sources of 8 cm radius along an 8 cm length path in terms of its height. Even though the maximum gain has decreased, we

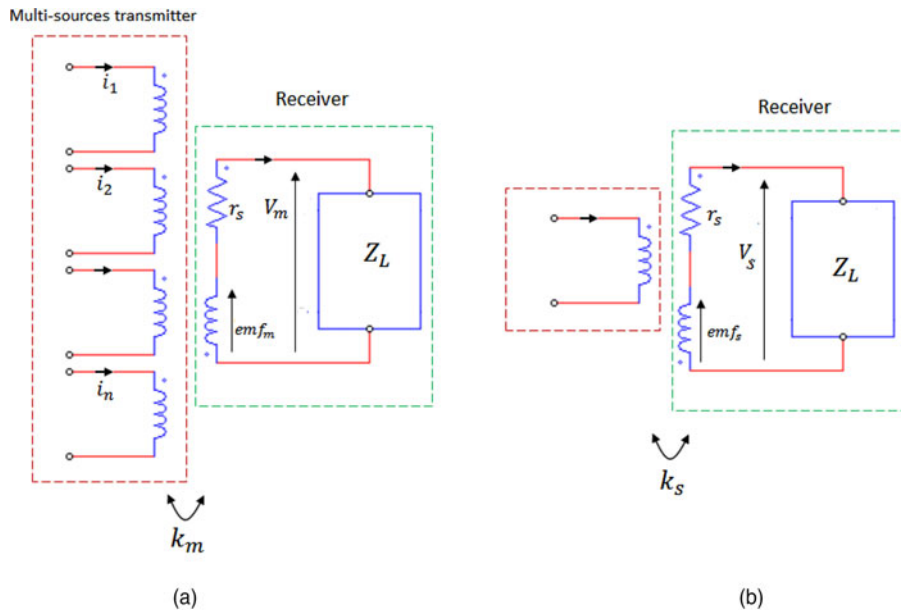


Fig. 7. (a) Schematic representation of the multi-source transmitter equivalent circuit, (b) schematic of conventional transmitter equivalent circuit.

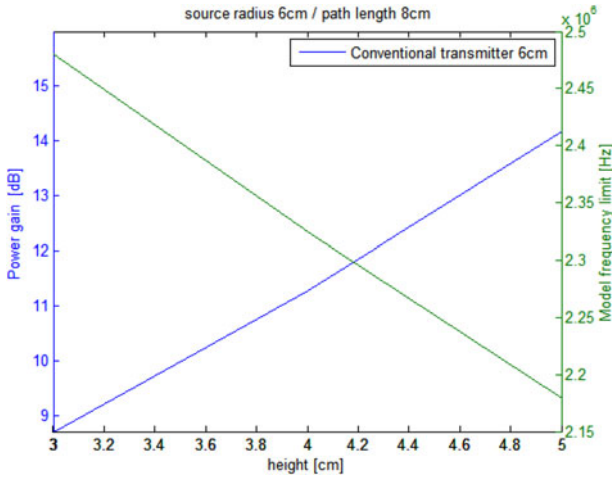


Fig. 8. Power gain for a multi-source transmitter of 6 cm radius over a path of 8 cm.

notice that a bigger source provides a more or less constant gain over the considered heights. The curve in red represents the power gain when the new current sum is injected within a conventional transmitter of a 6 cm radius. This curve shows that power transfer gain reaches 10 dB.

Figure 10 shows the gain evolution for a path length of 12 cm. it appears that using a transmitter containing sources of 6 cm radius does not provide a good enough gain. Indeed, when the receiver path is placed at 5 cm height, the gain is 0 which means that the multi-sources transmitter transfers the same power as a conventional single-source transmitter (Fig. 11). However, the transmitter containing sources with a radius of 8 cm provides an interesting power gain which enhances the power transfer up to 7.6 dB at 5 cm height. This result implies that for a longer path it is recommended to use a larger source. However, increasing the dimensions of the system every time the path gets longer may not be the best solution. This is why the association of different multi-source transmitters shown in Fig. 12 is suggested. Transmitters in such a configuration are activated alternatively depending on the receiver’s position. This way, a transmitter is turned ON when the receiver is

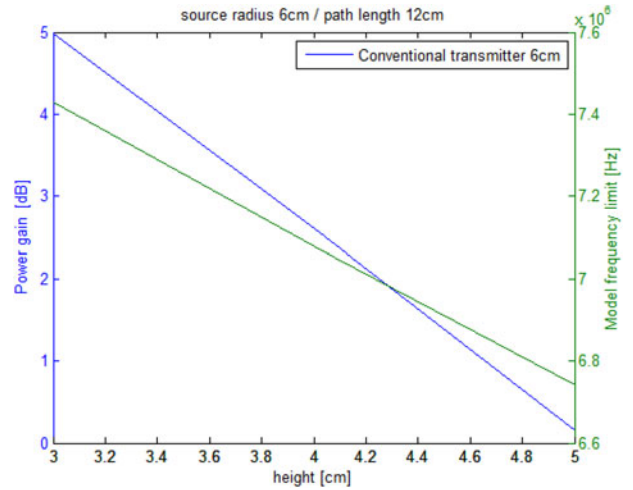


Fig. 10. Power gain for a multi-source transmitter of 6 cm radius over a path of 12 cm.

moving along its corresponding section. Thus, from the obtained results; an association of multi-source transmitters containing sources of 6 cm radius over an infinite length path; enhances the power transfer up to 5 dB (see Fig. 12).

## V. LOSS DISCUSSION

Even though the work presented here treats about transmitter’s design, it is worth it to mention that the transmitter in question does not affect the WPT system (converter + transmitter + receiver) overall efficiency. On the contrary, it helps to decrease it. If we consider resonant converters and where conduction losses represent a serious problem (switching losses being considerably reduced and considered negligible at high-power levels); this concept allows to considerably reduce them.

By considering that conduction losses depend on the current square, splitting the current through different sources will divide the total conduction losses by the number of sources (roughly) which makes the conduction losses much lower than in a conventional system.

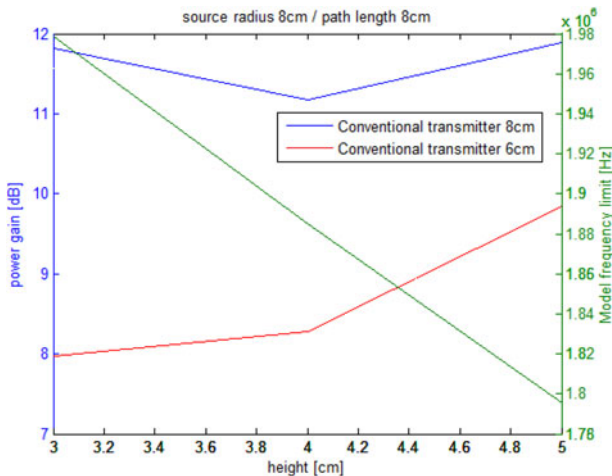


Fig. 9. Power gain for a multi-source transmitter of 8 cm radius over a path of 8 cm.

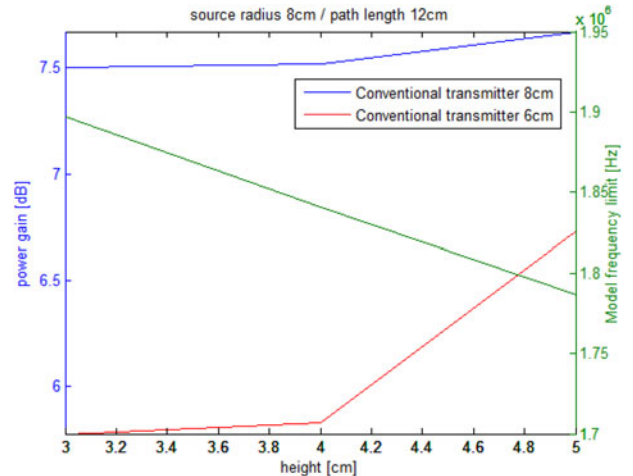


Fig. 11. Power gain for a multi-source transmitter of 8 cm radius over a path of 12 cm.



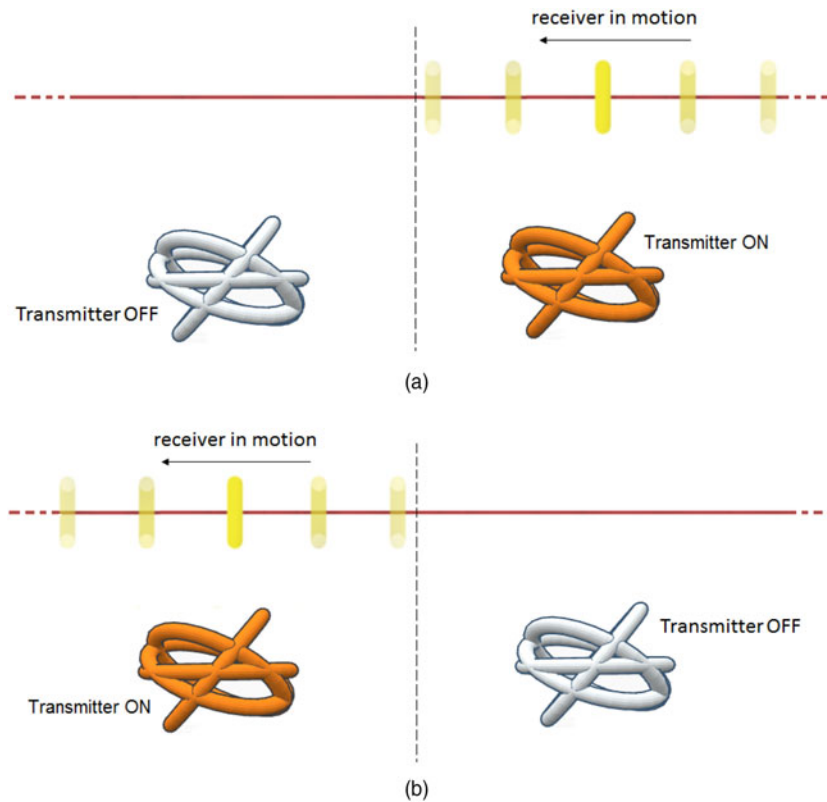


Fig. 12. Association with series of multi-source transmitters for an infinite length path.

This represents the other big advantage of the concept presented here and makes its implementation more interesting.

## VI. CONCLUSION

In this paper, a new type of transmitters dedicated to dynamic WPT in medical applications has been presented. Such multi-sources transmitters provide the needed magnetic field distribution in applications where transmitter-to-receiver orientation shift angles are constraining. For this purpose, an inverse problem-based characterization method has been used in order to deliver the required magnetic field along the receiver's path. The obtained transmitter design shows a significant power gain enhancement when compared with a conventional flat transmitter. A power gain of 14 dB has been obtained along a path of 8 at 5 cm height, while a gain of 5 dB at a height of 3 cm has been obtained for a path with an infinite length.

## ACKNOWLEDGEMENTS

The authors would like to thank Dr. A. Boushaba for his language assistance and proof reading.

## REFERENCES

- [1] Ryan, D.M.; LaFollette, R.M.; Salmon, L.: Microscopic batteries for micro electromechanical systems (MEMS), in *Proc. of the 32<sup>nd</sup> Intersociety Energy Conversion Engineering Conf., 1997. IECEC-97*, July–August 1997, **1**, 77–82.
- [2] Trevisan, R.; Costanzo, A.: State-of-the-art of contactless energy transfer (CET) systems: design rules and applications. *Wireless Power Transf.* **1** (2014), 10–20.
- [3] Visser, H.J.: A brief history of radiative wireless power transfer, in *11<sup>th</sup> European Conf. on Antenna and Propagation*, 2017, 327–330.
- [4] Ettorre, M.; Alomar, W.A.; Grbic, A.: Radiative wireless power transfer system using wideband, wide-angle slot arrays. *IEEE Trans. Antennas Propag.*, **65** (2017), 2975–2982.
- [5] Mohamed, A.A.S.; Mari, A.A.; Mohammed, O.A.: Magnetic design considerations of bidirectional inductive wireless power transfer system for EV applications. *IEEE Trans. Magn.*, **53** (6) (2017), 1–5.
- [6] Ravikiran, V.; Keshri, R.K.; Santos, M.M.: Inductive characteristics of asymmetrical coils for wireless power transfer, in *IEEE Int. Conf. on Industrial Technology*, 2017, 538–542.
- [7] Dai, J.; Ludois, D.C.: A survey of wireless power transfer and a critical comparison of inductive and capacitive coupling for small gap applications. *IEEE Trans. Power Electron.*, **30** (2015), 6017–6029.
- [8] Yi, K.H.: High frequency capacitive coupling wireless power transfer using glass dielectric layers, in *IEEE Wireless Power Transfer Conf.*, 2016, 1–3.
- [9] Waffenschmidt, E.; Staring, T.: Limitation of inductive power transfer for consumer applications, in *EPE '09 13<sup>th</sup> European Conf. on Power Electronics and Applications*, September 2009, 2009, 1–10.
- [10] Luo, Y.; Dahmardeh, M.; Chen, X.; Takahata, K.: A resonant-heating stent for wireless endohyperthermia treatment of restenosis. *Sens. Actuators A*, **236** (2015), 323–333.

- [11] Luo, Y.; Chen, X.; Dahmardeh, M.; Takahata, K.: RF-Powered stent with integrated circuit breaker for safeguarded wireless hyperthermia treatment. *J. Microelectromech. Syst.*, **24** (2015), 1293–1302.
- [12] Ye, D.; Yan, G.; Wang, K.; Ma, G.: Development of a micro-robot for endoscopes based on wireless power transfer. *Minim. Invasive Ther. Allied Technol.*, **17** (3) (2008), 181–189.
- [13] Lee, S.G.; Hoang, H.; Choi, Y.H.; Bien, F.: Efficiency improvement for magnetic resonance based wireless power transfer with axial-misalignment. *Electron. Lett.*, **48** (6) (2012), 339–340.
- [14] Wang, J.; Ho, S.L.; Fu, W.N.; Sun, M.: Analytical design study of a Novel Witricity charger with lateral and angular misalignments for efficient wireless energy transmission. *IEEE Trans. Magn.*, **47** (10) (2011), 2616–2619.
- [15] Jonah, O.; Georgakopoulos, S.V.; Tentzeris, M.M.: Orientation insensitive power transfer by magnetic resonance for mobile devices, in *Proc. 2013 IEEE Wireless Power Transfer*, Perugia, Italy, May 2013, 5–9.
- [16] Ng, W.M.; Zhang, C.; Lin, D.; Ron Hui, S.Y.: Two- and three-dimensional omnidirectional wireless power transfer. *IEEE Trans. Power Electron.*, **29** (9) (2014), 4470–4474.
- [17] Reinhold, C.; Scholz, P.; John, W.; Hilleringmann, U.: Efficient antenna design of inductive coupled RFID-systems with high power demand. *J. Commun.*, **2** (6) (2007), 14–23.
- [18] Beghou, L., Costa, F.; Pichon, L.: Detection of electromagnetic radiations sources at the switching time scale using an inverse problem-based resolution method – application to power electronic circuits. *IEEE Trans. Electromagn. Compat.*, **57** (1) (2015), 53–60.
- [19] Abramowitz, M.; Stegun, I.A.: *Handbook of Mathematical Functions with Formulas, Graphs, and Mathematical Tables*, Applied Mathematics Series 55, National Bureau of Standards, USA, June 1964.
- [20] Michalewicz, Z.: *Genetic Algorithms + Data Structures = Evolution Programs*. 3rd ed., Springer, New York, 1996. Revised and extended edition.



**Lotfi Beghou** received his engineering degree in power electronics and electromagnetics from the University of Constantine, Algeria, in 2005. He has received the MSc and the Ph.D. degrees from the university of Paris sud, France, in 2006 and 2012. He has worked as a postdoctoral researcher in power electronics and electromagnetics at Dartmouth College, University of North Carolina and University of British Columbia. His research interests include, applied electromagnetics, power electronics and electromagnetic compatibility.